Inhibition of diacylglycerol kinase α restores restimulation-induced cell death and reduces immunopathology in XLP-1

HHS Public Access

Author manuscript

Sci Transl Med. Author manuscript; available in PMC 2016 July 13.

Published in final edited form as:

Sci Transl Med. 2016 January 13; 8(321): 321ra7. doi:10.1126/scitranslmed.aad1565.

Inhibition of diacylglycerol kinase alpha restores restimulation-induced cell death and reduces immunopathology in XLP-1

Elisa Ruffo[1,†], **Valeria Malacarne**[1,†], **Sasha E. Larsen**[2,†], **Rupali Das**[3,†], **Laura Patrussi**[4], **Christoph Wülfing**[5], **Christoph Biskup**[6], **Senta M. Kapnick**[7], **Katherine Verbist**[8], **Paige Tedrick**[8], **Pamela L. Schwartzberg**[7], **Cosima T. Baldari**[4], **Ignacio Rubio**[9], **Kim E. Nichols**[8,#], **Andrew L. Snow**[2,#], **Gianluca Baldanzi**[1,#], and **Andrea Graziani**[1,10,#,*]

[1]Department of Translational Medicine and Institute for Research and Cure of Autoimmune Diseases, University of Piemonte Orientale, 28100 Novara, Italy

[2]Department of Pharmacology and Molecular Therapeutics, Uniformed Services University of the Health Sciences, Bethesda, MD 20814, USA

[3]Department of Physiology, Michigan State University, East Lansing, MI 48824, USA

[4]Department of Life Sciences, University of Siena, Siena, Italy

[5]School of Cellular and Molecular Medicine, University of Bristol, Bristol, UK

[6]Jena University Hospital, Biomolecular Photonics Group, D 07740 Jena, Germany

[7]Genetic Disease Research Branch National Human Genome Research Institute, National Institutes of Health, Bethesda, MD 20892, USA

[8]Department of Oncology, St. Jude Children's Research Hospital, Memphis, TN 38105 USA

[9]Integrated Research and Treatment Center, Center for Sepsis Control and Care and Institute of Molecular Cell Biology, Center for Molecular Biomedicine, Jena University Hospital, Jena, Germany

[10]School of Medicine, University Vita e Salute San Raffaele, Milan, Italy

Abstract

X-linked lymphoproliferative disease (XLP-1) is an often-fatal primary immunodeficiency associated with the exuberant expansion of activated $CD8^+$ T cells following Epstein-Barr virus (EBV) infection. XLP-1 is caused by defects in SAP, an adaptor protein that modulates T cell receptor (TCR)-induced signaling. SAP-deficient T cells exhibit impaired TCR restimulation-induced cell death (RICD) and diminished TCR-induced inhibition of diacylglycerol kinase alpha

*To whom correspondence should be addressed: School of Medicine, University Vita e Salute San Raffaele, Milan, Italy. graziani.andrea@hsr.it.

†These authors contributed equally to this work

#These authors contributed equally to this work

Author contributions: ER, VM, SEL, ALS, and GB designed and carried out *in vitro* experiments; RD, KV, PT and KEN *in vivo* experiments; SEL and ALS experiments on XLP-1 patient lymphocytes; VM, IR and CB imaging in Jurkat cells; LP and CTB imaging on primary lymphocytes, CW imaging on mouse lymphocytes, SMK and PLS cytotoxicity assays; GB, AG, KEN and ALS designed the project, supervised research and wrote the paper.

Competing interests: The authors declare no conflict of interest.

(DGKα), leading to increased diacylglycerol metabolism and decreased signaling through Ras and PKCθ. Here, we show that down-regulation of DGKα activity in SAP-deficient T cells restores diacylglycerol signaling at the immune synapse and rescues RICD via induction of the pro-apoptotic proteins NUR77 and NOR1. Importantly, pharmacological inhibition of DGKα prevents the excessive $CD8^+$ T cell expansion and IFNγ production that occur in Sap-deficient mice following Lymphocytic Choriomeningitis Virus infection without impairing lytic activity. Collectively, these data highlight DGKα as a viable therapeutic target to reverse the life-threatening EBV-associated immunopathology that occurs in XLP-1 patients.

Introduction

X-linked lymphoproliferative disease (XLP-1) is a heritable immune disorder caused by germline mutations in the *SH2D1A* gene, which encodes the Signaling Lymphocytic Activation Molecule (SLAM)-associated protein (SAP) (1). SAP is a small SH2 domain-containing adaptor primarily expressed in T, natural killer (NK) and invariant NKT (iNKT) cells (1). XLP-1 is best recognized for the increased susceptibility of affected males to develop overwhelming lymphoproliferation following primary Epstein Barr virus (EBV) infection (2). Also known as fulminant infectious mononucleosis (FIM), this lymphoproliferative process is characterized by the massive accumulation of activated $CD8^+$ T cells, which infiltrate multiple organs and inflict severe tissue damage. FIM is the most common and clinically challenging manifestation of XLP-1, with up to 65% of patients dying despite the use of chemo-immunotherapy (3). Accordingly, alternative and more effective treatment strategies are sorely needed for XLP-1 patients who develop FIM.

T lymphocytes derived from XLP-1 patients exhibit multiple functional defects, including reduced cytotoxic activity (4) and impaired restimulation-induced cell death (RICD) (5). RICD is a self-regulatory apoptosis program triggered by repeated TCR stimulation that maintains peripheral immune homeostasis by constraining the accumulation of activated T cells (6). A similar death defect is present in the activated T cells of *Sh2d1a*$^{-/-}$ mice (7). It is proposed that defective RICD, combined with impaired clearance of EBV-infected B cells, sustains and amplifies the expansion of activated T cells that typifies FIM (5, 6).

SAP binds to immunotyrosine-based switch motifs (ITSMs) within the cytoplasmic domains of the SLAM-family receptors (SLAM-Rs) (8), thus competing with the binding of SH2 domain containing inhibitory lipid and tyrosine phosphatases such as SHIP and SHP-1/SHP-2 (9). In addition, SAP facilitates recruitment of kinases such as FynT and Lck to SLAM-Rs to promote optimal signaling within T, NK and NKT cells (10, 11). Indeed, RICD resistance in XLP patient T cells results in part from weak TCR signaling associated with excess SHP-1 activity and defective recruitment of Lck to the NTB-A receptor, which colocalizes with the TCR (5, 11). Although SAP links SLAM-R signaling to several downstream functions via activation of Src-family kinases (e.g. IL-4 secretion (12), iNKT cell development (13)), this signaling axis is not the only pathway in which SAP is involved for signal regulation. For example, the requirement for SAP in the provision of $CD4^+$ T cell-mediated "help" for B cell differentiation is Fyn-independent (14). To fully understand XLP-1 pathogenesis and develop more effective therapeutic interventions, the mechanistic

characterization of signaling molecules involved in these “alternative” SAP-dependent signaling pathways is imperative.

We recently observed that following TCR stimulation, SAP selectively inhibits diacylglycerol kinase-alpha (DGKα) without requiring FynT or Lck (15). DGKα and DGKζ phosphorylate diacylglycerol (DAG) to generate phosphatidic acid, thereby modulating TCR signal strength by regulating DAG levels and downstream biochemical events (16, 17). In activated T cells, silencing SAP expression results in persistently active DGKα and thus impaired DAG signaling, leading to reduced-mediated PKCθ membrane recruitment, NFAT and ERK1/2 activation and interleukin 2 (IL-2) production (15). These data collectively suggest that upon antigen stimulation, SAP inhibits DGKα activity to facilitate optimal DAG accumulation and full TCR signal strength, ultimately leading to cell activation.

Because TCR signal strength directly correlates with RICD sensitivity (18), we hypothesized that the reduced RICD of XLP-1 T cells might be linked to deregulation of DGKα in the absence of functional SAP. Consistent with this notion, we show herein that the loss of SAP in T cells results in reduced DAG polarization to the immune synapse (IS) and impaired TCR-induced DAG-dependent TCR signaling. Both of these events are due to persistent DGKα activity and contribute to RICD resistance. Consequently, the inhibition of DGKα in XLP-1 T cells restored DAG signaling and RICD by rescuing IS architecture and triggering a specific DAG-dependent apoptotic process mediated by the orphan receptors *NR4A1* (NUR77) and *NR4A3* (NOR1). Strikingly, *in vivo* inhibition of DGKα activity reduced the excessive $CD8^+$ T cell accumulation and IFNγ production that occur in *Sh2d1a*$^{-/-}$ mice infected with Lymphocytic Choriomeningitis Virus (LCMV), a murine model of FIM. Our findings illuminate the SAP/DGKα signaling axis as a key regulator of TCR-induced apoptosis. Importantly, these results highlight DGKα as a novel, druggable target for treating FIM by promoting RICD, reducing the accumulation of pathogenic, activated $CD8^+$ T cells and thus mitigating the life-threatening immunopathology that often occurs in EBV-infected XLP-1 patients.

Results

DGKα inhibition rescues RICD in SAP-deficient T cells

To investigate whether reduced DAG signaling contributes to the T cell-driven pathologic manifestations of XLP-1, we examined whether silencing or inhibition of DGKα could restore the sensitivity of XLP-1 T cells to RICD. SAP-deficient XLP-1 T cells exhibit reduced RICD relative to control T cells following stimulation with increasing concentrations of the agonistic anti-CD3 Ab OKT3 (5) (Fig 1A–B). Remarkably, this defect in RICD was substantially rescued by the siRNA-mediated silencing of DGKα (Fig. 1A–C), or by pre-treatment with the DGKα inhibitors R59949 (Fig. 1D–E) or R59022 (Fig. 1F) (19). The rescue in RICD obtained upon DGKα inhibition was likely due to the induction of apoptosis, as indicated by an increased percentage of $AnnexinV^+$ cells (Fig. 1G). Conversely, the inhibition or silencing of DGKα had little effect on RICD in activated T cells from healthy subjects (Fig. 1–2).

As patient-derived cells were limited, we repeated these assays using siRNA to knock down SAP expression in activated T cells from healthy donors (Fig. 2) (5). In agreement with our prior findings, SAP-silenced cells exhibited defective RICD that was rescued by concomitant silencing of DGKα (Fig. 2A–B), or by treatment with the DGKα inhibitors R59949 (Fig. 2C) or R59022 (Fig. 2D). This restoration of RICD in SAP-silenced T cells was associated with enhanced apoptosis, as indicated by increased AnnexinV staining (Fig. 2E). For other isoforms expressed in T cells, silencing of DGKζ, but not DGKδ, also partially rescued RICD in SAP silenced cells (Fig. S1A–D). Conversely, overexpression of DGKα or DGKζ conferred partial resistance to RICD in normal T cells (Fig. S1E–F). These findings suggest a link between the RICD resistance of SAP-deficient lymphocytes and unrestrained DAG depletion caused by enhanced DGK activity. To explore this further, we supplemented cultures with the DAG analogue 1,2-dioctanoyl-sn-glycerol (C8-DAG), which is rapidly incorporated into the cell membrane and triggers DAG-dependent signaling (20). Indeed, C8-DAG treatment markedly enhanced RICD in SAP-silenced but not control T cells (Fig. 2F). Collectively, these data demonstrate that excessive DGKα activity contributes to RICD resistance in SAP-deficient T cells, and that this process can be reversed by inhibition of DGKα. These data suggest that SAP promotes TCR signal strength and RICD sensitivity by attenuating DAG metabolism carried out by DGKα in activated T cells (Fig. 2G).

Inhibition of DGKα rescues defective DAG polarization and signaling at the IS in SAP-deficient cells

DAG generation and polarization at the IS are required for TCR-induced cellular responses (21). To investigate whether the deregulated DGKα activity caused by SAP deficiency affects DAG polarization toward the IS, we imaged DAG localization using a PKCθ-CRD-based biosensor (22). Following activation by superantigen-loaded Raji B cells, we observed that PKCθ-CRD polarization to the IS was strongly reduced in SAP-silenced versus control Jurkat cells (Fig. 3A–D). In contrast, co-silencing of DGKα (Fig. 3A, B) or pre-treatment with the DGK inhibitor R59949 (Fig. 3C, D) restored PKCθ-CRD polarization in SAP-silenced T cells. Consistent with the finding that DGKα shapes the DAG gradient at the IS (23), DAG polarization was also reduced in SAP-expressing, DGKα-silenced Jurkat cells (Fig. 3A, B).

Polarized DAG signaling triggers F-actin polymerization and microtubule organizing center (MTOC) orientation (24, 39). Consistent with reduced DAG polarization, SAP-silenced T cells exhibited a strong defect in F-actin accumulation at, and MTOC orientation toward, the IS upon contact with superantigen-loaded Raji cells (Fig. 3E–J). Again, silencing or inhibition of DGKα partially restored these processes (Fig. 3E–J). These findings indicate that SAP regulates the architecture of the IS by inhibiting DGKα, thereby limiting DAG metabolism locally.

We next investigated whether inhibition of DGKα restores DAG-mediated signaling downstream of the TCR in SAP-silenced primary human T cells. PKCθ and RasGRP1 are recruited to the IS in a DAG-dependent manner (25, 26), and are required for induction of RICD (27, 28). Consistent with our hypothesis, SAP-silenced primary T cells exhibited

defective recruitment of PKCθ and RasGRP1 to the IS, which was fully restored upon DGKα silencing (Fig. 4A–B, E–F) or pharmacological inhibition (Fig. 4C–D, G–H). Considering inhibition of DGKα also rescues defective ERK1/2 activation in SAP-deficient T cells (15), these data underscore the importance of the SAP/DGKα axis in regulating DAG-dependent signaling.

To test if inhibition of DGKα rescues RICD in SAP-deficient T cells by restoring specific DAG-mediated signaling pathways, we examined whether the rescue of RICD requires the activity of PKCθ or RasGRP1. Silencing of PKCθ (Fig. 5A) or RasGRP1 (Fig 5B) reduced RICD in control siRNA transfected T cells, and completely abrogated the rescue of RICD in SAP and DGKα siRNA transfected cells. Moreover, pharmacological inhibition of PKC or MEK/ERK enzymatic activity also prevented the restoration of RICD noted following DGKα silencing in SAP-deficient T cells (Fig. S2).

TCR activation stimulates DAG-dependent induction of IL-2 and the high-affinity IL-2 receptor CD25 (29, 30), which are both required for RICD (31). Indeed, inhibition or silencing of DGKα restored induction of CD25 in SAP-silenced T cells after TCR restimulation, and a similar trend was observed with IL-2 expression (Fig. 5C–E). These findings further establish the SAP/DGKα signaling axis as a critical regulator of DAG signaling potency. Collectively, these findings underscore the vital role of SAP-dependent inhibition of DGKα in sustaining DAG signaling, leading to the activation of PKCθ and Ras-ERK and RICD (Fig. 5F).

NUR77 and NOR1 mediate the rescue of RICD that is induced by DGKa inhibition in SAP-deficient T cells

We next investigated the mechanism by which the enhancement of DAG signaling obtained following inhibition of DGKα restores RICD sensitivity in SAP-deficient T cells. We previously showed that in SAP-deficient T cells, TCR-induced expression of key pro-apoptotic genes such as *FASLG* and *BCL2L11* is impaired (5). Surprisingly, we observed that silencing or inhibition of DGKα failed to rescue *FASLG* or *BCL2L11* expression following TCR restimulation of SAP-silenced T cells (Fig. S3A, B). Similarly, DGKα blockade failed to restore the induction of all three major isoforms of BIM protein (extra-long EL, long L, and short S), as well as full-length and soluble FASL protein in SAP-silenced and XLP-1 patient T cells following restimulation (Fig. S3C–E). These observations imply that DGKα inhibition does not restore all SAP-dependent, pro-apoptotic effector functions that contribute to RICD sensitivity.

Instead, we found that SAP-deficient T cells exhibit a previously unrecognized defect in TCR restimulation-induced upregulation of *NR4A1* (NUR77) and *NR4A3* (NOR1), two nuclear receptors involved in negative selection of thymocytes and RICD of mature T cells (32). Importantly, DGKα silencing or inhibition selectively restored TCR-dependent induction of both *NR4A1* and *NR4A3* in SAP-silenced activated T cells (Fig. 6A–D). DGKα inhibition also partially rescued NUR77 and NOR1 protein induction in XLP-1 T cells following TCR restimulation (Fig. 6E). Upon TCR engagement, NUR77 and NOR1 proteins are phosphorylated by the ERK1/2-regulated 90 kD ribosomal S6 kinase (RSK), triggering the intrinsic apoptosis pathway (33). Indeed, the RSK-specific inhibitor SL0101

(34) significantly reduced RICD in control T cells, confirming that phosphorylation of NUR77 and NOR1 is an important component of RICD execution (Fig 6F–H). Importantly, SL0101 significantly blunted the RICD rescue triggered by DGKα inhibition in XLP-1 T cells, as well as in SAP/DGKα-silenced T cells (Fig 6F–H). These data indicate that the rescue of RICD afforded by DGKα blockade in SAP-deficient T cells is dependent on RSK activity. Moreover, concomitant knockdown of NUR77 and NOR1 reduced the rescue of RICD induced by DGKα inhibition in XLP-1 T cells (Fig. 6I–K). Altogether, these observations indicate that inhibition of DGKα boosts RICD in SAP-deficient T cells in part by selectively restoring TCR-induced upregulation and RSK-dependent phosphorylation of NUR77 and NOR1 (Fig. 6L).

DGKα inhibition reduces CD8$^+$T cell accumulation and activation in LCMV-infected Sh2d1a$^{-/-}$ mice

Defective RICD is thought to contribute to the aberrant T cell activation and accumulation that occur in EBV-infected XLP-1 patients (35). The demonstration that DGKα silencing or inhibition sensitizes SAP-deficient lymphocytes to RICD *in vitro* prompted us to assess whether DGKα inhibition might influence T cell-mediated immunopathology *in vivo*. Towards this end, we used a murine model in which *Sh2d1a*$^{-/-}$ mice are infected with LCMV. In this model, *Sh2d1a*$^{-/-}$ mice develop many of the cardinal manifestations of FIM, including CD8$^+$ T cell expansion, pro-inflammatory cytokine production and tissue infiltration (36, 37). For these experiments, wild-type (WT; *Sh2d1a*$^{+/+}$) or *Sh2d1a*$^{-/-}$ mice were infected with LCMV-Armstrong and 4 days later, treated with vehicle or R59022 (38). On day 8, the peak of the anti-viral T cell response, mice were euthanized and evaluated for hyper-inflammation.

Following LCMV infection, both WT and S*h2d1a*$^{-/-}$ mice developed marked and comparable splenomegaly (Fig 7A–B) that was associated with an increase in the absolute number of total splenocytes (Fig. 7C). Examination of splenocyte immunophenotype revealed a significant increase in the percentage and absolute number of total as well as LCMV-specific (gp33$^+$) CD8$^+$ T cells, the majority of which exhibited an activated CD44$^+$ phenotype (Fig. 7D–I). Treatment of LCMV-infected WT mice with R59022 did not significantly affect any of these parameters (Fig. 7). Conversely, R59022 treatment of LCMV-infected *Sh2d1a*$^{-/-}$ mice appeared to lessen organomegaly (Fig. 7A–B) and decrease the total splenic lymphocyte count (Fig. 7C). Although R59022 treatment did not affect the percentage of activated splenic CD8$^+$ T cells in either mouse strain, it did induce a significant decrease in the number of total as well as LCMV-specific CD8$^+$ T cells selectively in the *Sh2d1a*$^{-/-}$ animals (Fig. 7D–I).

Compared to WT animals, LCMV-infected S*h2d1a*$^{-/-}$ mice also exhibited a trend toward higher serum IFNγ levels (Fig. 8A) and greater degrees of tissue inflammation (Fig 8B–D). To evaluate whether DGKα inhibition affected CD8$^+$ T cell functions such as cytokine production or degranulation, splenocytes from LCMV-infected mice were cultured directly *ex vivo* with the MHC class I restricted LCMV peptide gp33 and examined for expression of intracellular TNFα, IFNγ and CD107α. Interestingly, R59022 treatment did not affect the percentage of CD8$^+$ T cells that secreted cytokines (TNFα or IFNγ) or degranulated

(CD107α exposure) in LCMV-infected WT or *Sh2d1a*$^{-/-}$ mice (Fig 8E–F). In fact, R59022 treatment actually enhanced the cytolytic activity of *Sh2d1a*$^{-/-}$ CD8^{+} T cells against autologous B cell targets *in vitro* (Fig. S5). However, such treatment did reduce the absolute number of cytokine producing and degranulating cells only in the *Sh2d1a*$^{-/-}$ animals (Fig. 8G). Consistent with these findings, only R59022-treated *Sh2d1a*$^{-/-}$ mice exhibited a significant reduction in the serum IFNγ levels (Fig 8A). Finally, R59022 treatment significantly reduced the number and size of hepatic inflammatory infiltrates in LCMV-infected *Sh2d1a*$^{-/-}$ but not WT mice (Fig 8B–D). These findings collectively indicate that inhibition of DGKα selectively decreases the magnitude of the CD8^{+} T cell effector pool in LCMV-infected *Sh2d1a*$^{-/-}$ mice. DGKα inhibition had no adverse effects on viral clearance, as LCMV was efficiently cleared from WT and *Sh2d1a*$^{-/-}$ mice by day 8 with or without R59022 treatment (Fig. S6). These pre-clinical data suggest that pharmacologic inhibition of DGKα might reduce the accumulation of aberrantly activated CD8^{+} T cells and subsequent hypercytokinemia and tissue inflammation that occur in EBV-infected XLP-1 patients, without impairing CD8^{+} T cell activity or viral clearance.

One major limitation of this study is its focus on the role of the SAP/DGKα axis strictly in T cells. It does not address the putative role of DGKα in other SAP-deficient immune cells such as NK or NKT cells, which also likely contribute to the development of various XLP-1 manifestations. In addition, although LCMV-infection of *Sh2d1a*$^{-/-}$ mice is a widely used murine model of FIM, it does not fully recapitulate the pathogenesis of EBV infection in humans. Finally, the translation of these findings to the clinic will require the development and characterization of novel, clinical-grade DGKα specific inhibitors. Nonetheless, our data clearly provide proof of concept that DGKα may be a novel drug target for treating XLP-1-associated FIM.

Discussion

Our results demonstrate that inhibition of DGKα restores sensitivity to RICD in SAP-deficient T cells and reduces hyper-inflammation in LCMV-infected *Sh2d1a*$^{-/-}$ mice. These data support the hypothesis that in SAP-deficient T cells, persistent DGKα activity increases DAG metabolism at the IS, thus reducing DAG signaling and RICD sensitivity, and underscore the role of SAP in modulating DGKα activity (15). In SAP-expressing T cells, further inhibition of DGKα only marginally influenced sensitivity to RICD *in vitro,* and did not dampen the LCMV-induced CD8^{+} T cell response of wild-type mice *in vivo*.

Our finding that inhibition of DGKα restores proper IS organization in SAP-deficient T cells indicates that SAP, through regulation of DGKα, controls DAG polarization at the IS, thus promoting F-actin polymerization and MTOC orientation. Indeed, DGKα is recruited to the pSMAC, where it shapes the DAG gradient responsible for the recruitment of novel PKC isoforms (ε, η and θ), which control MTOC polarization and actin polymerization (Fig. 3) (23, 39). DGKα inhibition also partially rescued impaired cytolytic activity in SAP-deficient CTLs (Fig. S5), further highlighting the link between SAP-dependent inhibition of DGKα and IS function (4). Altogether, these data indicate that SAP-mediated negative regulation of DGKα controls IS structural organization and function by regulating the TCR-induced gradient of DAG.

Both DGKα and DGKζ regulate TCR-induced DAG-signaling (16, 17). Consistently, inhibition or overexpression of either isoform rendered T cells more or less sensitive to RICD, respectively, confirming that both isoforms regulate DAG signalling in this context (Fig S1). Accordingly, administration of exogenous DAG partially rescued the defective RICD in SAP-deficient T cells (Fig 2F). However, only DGKα is regulated by SAP and shapes the DAG gradient at the IS (15, 23). We speculate that DGKα, which co-localizes with F-actin at the pSMAC, regulates the DAG gradient and F-actin polymerization at the IS, whereas DGKζ, which is more evenly distributed in the IS, metabolizes most of DAG generated there, consistent with proposed models (23, 40). Notably silencing of DGKδ, which is highly expressed in T cells, did not affect RICD, underscoring the specific roles of DGKα and DGKζ in regulating the DAG pool relevant for signaling and RICD onset.

Our finding that inhibition of DGKα restored RasGRP1 and PKCθ recruitment to the IS in SAP-deficient T cells, and subsequent DAG-dependent induction of IL-2 and CD25, illuminates a biochemical link between the SAP/DGKα axis, IS restoration, and downstream signaling events required for RICD (27–30). Indeed, activation of RasGRP1 and PKCθ was required to rescue RICD in SAP-deficient T cells upon DGKα blockade (Fig. 5A–B, S2). Interestingly, DGKα inhibition cannot recapitulate all SAP-dependent signaling functions, such as TCR-induced expression of *FASLG* or *BCL2L11*, genes previously implicated in SAP-associated induction of RICD (5). This observation suggests that rescue of DAG-mediated signaling activates other pro-apoptotic pathways that partially compensate to boost RICD sensitivity. Here we show that the induction of NUR77 and NOR1 is defective in TCR-restimulated SAP-deficient T cells, and that the expression of these genes is restored by inhibition of DGKα. NUR77 and NOR1 are orphan nuclear receptors known to trigger thymocyte apoptosis during negative selection, and mediate RICD (32, 41). The pro-apoptotic activity of NUR77 and NOR1 depends on their phosphorylation by RSK, an ERK-1/2 dependent kinase, and subsequent translocation to the mitochondria to promote mitochondrial depolarization and apoptosis (32, 33). We observed that ERK and RSK activity, as well as NUR77 and NOR1, were required for RICD rescue triggered by DGKα inhibition in XLP-1 T cells. These observations provide a mechanistic connection between the rescue of DAG signaling and execution of RICD.

EBV-induced FIM is proposed to result from defective RICD of $CD8^+$ T cells and impaired cytotoxic elimination of EBV-infected B cells by $CD8^+$ T cells and NK cells. These events contribute to the excessive accumulation of activated effector $CD8^+$ T cells and life-threating damage to the liver, bone marrow, and other organs (2, 5). Using a murine model of FIM (36, 37), we showed that DGKα inhibition had no significant effect on reducing the activation status or function (e.g. cytokine secretion or degranulation) of effector $CD8^+$ T cells in either WT or *Sh2d1a*$^{-/-}$ mice. These data suggest that treatment with R59022 after LCMV infection does not impair initial lymphocyte activation. However, this treatment did significantly decrease the absolute number of activated $CD8^+$ T cells in *Sh2d1a*$^{-/-}$ mice, leading to fewer and smaller lymphocytic infiltrates within the liver and marked reductions in the level of IFNγ in the serum. These results suggest that RICD resistance is connected to aberrant DGKα activity and serves as a key driver of virus-induced immunopathology in *Sh2d1a*$^{-/-}$ mice. Remarkably, the apoptosis resistance of activated T cells in LCMV-infected *Sh2d1a*$^{-/-}$ mice can be overcome via DGKα inhibition, even when such inhibition is

initiated well after infection is established. These data are relevant to the clinical setting, where patients often present with FIM days to weeks after primary EBV infection.

In conclusion, our findings underscore the importance of SAP-mediated DGKα inhibition in maintaining lymphocyte homeostasis by ensuring sufficient TCR-induced DAG signaling strength for apoptosis. These data provide proof of principle that treatment with a DGKα inhibitor could serve as a novel, reasonable strategy to counteract pathological EBV-driven lymphohistiocytosis that occurs in EBV-infected XLP-1 patients by restoring the RICD sensitivity of activated $CD8^+$ T cells.

Materials and Methods

Study design

This was a preclinical study to 1) determine if DGKα inhibition could rescue RICD in SAP-deficient T cells, and 2) assess the efficacy of a DGKα inhibitor in attenuating $CD8^+$ T cell lymphocytosis and immunopathology in LCMV-infected SAP-deficient mice, a model of FIM. Although *in vitro* experiments utilizing XLP-1 patient T cells were often constrained by limited sample availability, each RICD experiment was performed with at least 2 separate XLP patients and different control donors (e.g. Fig 1A–B). We also generated robust corroborating data using siRNA-mediated SAP knockdown in T cells from multiple human donors ($n \geq 3$ experiments each). Once we established that DGKα blockade restored RICD sensitivity in SAP-deficient T cells, we focused on delineating the biochemical mechanism that explains this phenomenon. For all *in vitro* data, the number of experiments (including technical replicates) is defined in each figure legend. For *in vivo* experiments, numbers of mice are outlined in each figure legend. All statistical analyses described below were verified by consultation with an experienced biostatistician (Cara Olsen, USUHS).

Cell culture

Peripheral blood mononuclear cells (PBMCs) were isolated from normal controls or XLP-1 patients by Ficoll-Paque PLUS (GE Healthcare) density gradient centrifugation, washed, and resuspended at 2×10^6 cell/ml in complete media (cRPMI): RPMI-GlutaMAX (Life Technologies) containing 10% heat inactivated FCS (Lonza), 2 mM glutamine, and 100 U/ml of penicillin and streptomycin (Life Technologies). T cells were activated with 1 μg/ml anti-CD3 (clone UCHT1) and anti-CD28 (clone CD28.2) antibodies. After 3 days, activated T cells were washed and cultured in cRPMI plus 100 IU/ml rhIL-2 (Peprotech) at 1.2×10^6 cells/mL for ≥7 days before apoptosis assays were conducted (media changed every 2–3 days).

Jurkat A3 cells were from ATCC, and 293FT from Life Technologies. Cells were cultured in RPMI or DMEM (Life Technologies) with 10% FCS and antibiotics/antimycotics (Sigma-Aldrich).

DGK inhibitors R59949 and R59022 (Sigma-Aldrich) were dissolved in DMSO; all reagents and antibodies used are listed in Table S1.

siRNA transfections

PBMCs were transfected with 200 pmol of Stealth Select siRNA or Stealth RNAi Negative Control Duplexes (Life Technologies). siRNA sequences are listed in Table S2. Transient transfections were performed using Amaxa nucleofector kits for human T cells (Lonza) and the Amaxa Nucleofector II or 4D systems (programs T-20 or EI-115). Cells were cultured in IL-2 (100 IU/ml) for 4 days to allow target gene knockdown. Knockdown efficiency was periodically evaluated by RT-PCR and Western blotting.

Conjugation and live-cell imaging of Jurkat T-cells

Jurkat T cells and Raji B cells were labeled, imaged and analyzed as described in the Supplemental Methods.

Immunofluorescence experiments with primary T cells

Human T cells were stimulated with soluble anti-CD3 and anti-CD28 (1 μg/ml) for at least 7 days and transfected with Amaxa Nucleofector™ Kit for human T Cells (Lonza) with control, SAP-specific and/or DGKα-specific siRNA. After 72 hours T cells were incubated with Raji B cells loaded with mixed SEE and SEB superantigens (1 μg/ml) for 15 min, fixed and stained for either PKCθ or RasGRP1. For some experiments, transfected T cells were pre-treated with R59949 (10 μM, 30 min 37°C) or DMSO before conjugation.

Cytofluorimetry

To examine RICD, activated T cells (10^5 cells/well) were plated in triplicate in 96-well round-bottom plates and treated with anti-CD3ε mAb OKT3 (1–100 ng/ml) in cRPMI + 100 IU/ml rhIL-2 for 24 hours. R59949 (5–10 μM), R59022 (5–10 μM), DAG (50 μM), U0126 (5 μM), FR180204 (10 μM) or Rottlerin (6 μM) inhibitors were added 30 minutes before restimulation. At 24 hours post-restimulation, cells were stained with 1 μg/ml propidium iodide and collected for 30 seconds per sample on FACScan or Accuri C6 flow cytometers (BD). Cell death was analyzed with CellQuest/CFlow software (BD) or Flowing software (Turku Bioimaging) as percentage of cell loss = (1 − [number of viable cells (treated) / number of viable cells (untreated)]) × 100 (5).

For AnnexinV assays, ~1×10^6 cells were treated with OKT3 (10 ng/ml) as above. Cells were stained 6–12 hours later with AnnexinV-PE (Biolegend) and analyzed on an Accuri C6.

To evaluate CD25 expression, 1×10^6 cells were stimulated with OKT3 (100 ng/ml) for 24 hours, fixed and stained with anti-CD25 plus anti-mouse AlexaFlour488. Stained cells were collected on a FACSCalibur.

Western blotting

Lymphocytes (1–10×10^6 cells) were stimulated, lysed and subjected to SDS-PAGE and immunoblotting as described (5, 15). Immunoblot images were acquired and quantified using a Versadoc Model 4000 Imaging System (Bio-Rad) or ImageJ software (for film). Spot densitometry analyses are summarized in Table S4.

Quantitative RT-PCR

Activated lymphocytes (30×10^6 cell/ml) were stimulated in cRPMI with 10 μg/ml OKT3 for 4 hours. R59949 (5 μM) was added 30 minutes before restimulation. Cells were washed with cold PBS, and mRNA was extracted using a ChargeSwitch Total RNA Cell Kit (Life Technologies). RNA was reverse transcribed using High-Capacity cDNA Reverse Transcription Kits (Life Technologies), and cDNA targets quantified by RT-PCR (C1000 Thermal Cycler CFX96, Bio-Rad) using TaqMan gene expression assays (see Table S3), with *GUSB* as the housekeeping control (Life Technologies).

Mice and in vivo experiments

Sh2d1a$^{-/-}$ mice were as described (37). C57BL/6 (B6) mice were purchased from Jackson Laboratories. To establish LCMV infection, mice received 2×10^5 plaque-forming units (PFU) of LCMV-Armstrong by intraperitoneal (i.p) injection on day 0 and experiments were carried out until day +8 post-infection. Beginning at day 4, mice were given twice daily i.p injections of R59022 at a dose of 2 mg/kg body weight, dissolved in DMSO. Mice in all groups were sex and age matched. Stimulation of mouse splenocytes *in vitro*, assessment of liver histology, and quantification of viral titers were performed as described in the Supplemental Methods.

Statistical analysis

Evaluation of *in vitro* assays across multiple treatments (RICD, RT-PCR, ELISA), and *in vivo* experiments, were analyzed using two-way ANOVA (alpha: 0.05) with Sidak's multiple comparisons correction using GraphPad PRISM software. When comparing two groups (RT-PCR, AnnV$^+$ cells), a two-tailed paired Student's t-test was performed in Microsoft Excel. Error bars are described in figure legends as ± SEM or ± SD where appropriate. A single asterisk denotes significance of a p-value ≤0.05 in all experiments; p-values are included in Table S5.

Study approval

Blood samples were obtained with informed consent under protocols approved by the respective Institutional Review Boards (Cincinnati Children's Hospital Medical Center, National Institute of Allergy and Infectious Diseases, University of Piemonte Orientale). Experimental procedures on animals were approved by the Institutional Animal Care and Use Committee at The Children's Hospital of Philadelphia and St. Jude Children's Research Hospital.

Supplementary Material

Refer to Web version on PubMed Central for supplementary material.

Acknowledgments

We thank the patients and their families for participating in our study. We also thank biostatistician Cara Olsen (USUHS) for consultation on statistical analysis, John Wherry for providing LCMV and assistance with performing LCMV infections, Doreen Cantrell for supplying the PKCθ-CRD construct, Roland Wedlich-Soldner for supplying the Lifeact-GFP construct and Julian Downward for supplying GFP-tubulin.

Funding: KN was supported by the XLP Research Trust and the Sean Fischel Fund for HLH Research. ALS and SEL were supported by grants from the NIH (1R01GM105821), XLP Research Trust, and USUHS. AG, ER, and VM were supported by grants from Telethon (GGP10034 and GGP13254) and AIRC (IG13524 and IG5392). GB is supported by University Piemonte Orientale (Young Investigators). VM was supported by a grant from the Compagnia di San Paolo. RD was supported by a NIH K22 grant (1 K22 CA188149-01).

References and Notes

1. Nichols KE, Harkin DP, Levitz S, Krainer M, Kolquist KA, Genovese C, Bernard A, Ferguson M, Zuo L, Snyder E, Buckler AJ, Wise C, Ashley J, Lovett M, Valentine MB, Look AT, Gerald W, Housman DE, Haber DA. Inactivating mutations in an SH2 domain-encoding gene in X-linked lymphoproliferative syndrome. Proc Natl Acad Sci U S A. 1998; 95:13765–13770. [PubMed: 9811875]
2. Tangye SG. XLP: clinical features and molecular etiology due to mutations in SH2D1A encoding SAP. J Clin Immunol. 2014; 34:772–779. [PubMed: 25085526]
3. Booth C, Gilmour KC, Veys P, Gennery AR, Slatter MA, Chapel H, Heath PT, Steward CG, Smith O, O'Meara A, Kerrigan H, Mahlaoui N, Cavazzana-Calvo M, Fischer A, Moshous D, Blanche S, Pachlopnik Schmid J, Pachlopnick-Schmid J, Latour S, de Saint-Basile G, Albert M, Notheis G, Rieber N, Strahm B, Ritterbusch H, Lankester A, Hartwig NG, Meyts I, Plebani A, Soresina A, Finocchi A, Pignata C, Cirillo E, Bonanomi S, Peters C, Kalwak K, Pasic S, Sedlacek P, Jazbec J, Kanegane H, Nichols KE, Hanson IC, Kapoor N, Haddad E, Cowan M, Choo S, Smart J, Arkwright PD, Gaspar HB. X-linked lymphoproliferative disease due to SAP/SH2D1A deficiency: a multicenter study on the manifestations, management and outcome of the disease. Blood. 2011; 117:53–62. [PubMed: 20926771]
4. Zhao F, Cannons JL, Dutta M, Griffiths GM, Schwartzberg PL. Positive and negative signaling through SLAM receptors regulate synapse organization and thresholds of cytolysis. Immunity. 2012; 36:1003–1016. [PubMed: 22683123]
5. Snow AL, Marsh RA, Krummey SM, Roehrs P, Young LR, Zhang K, van Hoff J, Dhar D, Nichols KE, Filipovich AH, Su HC, Bleesing JJ, Lenardo MJ. Restimulation-induced apoptosis of T cells is impaired in patients with X-linked lymphoproliferative disease caused by SAP deficiency. J Clin Invest. 2009; 119:2976–2989. [PubMed: 19759517]
6. Snow AL, Pandiyan P, Zheng L, Krummey SM, Lenardo MJ. The power and the promise of restimulation-induced cell death in human immune diseases. Immunol Rev. 2010; 236:68–82. [PubMed: 20636809]
7. Chen G, Tai AK, Lin M, Chang F, Terhorst C, Huber BT. Increased proliferation of CD8+ T cells in SAP-deficient mice is associated with impaired activation-induced cell death. Eur J Immunol. 2007; 37:663–674. [PubMed: 17266174]
8. Poy F, Yaffe MB, Sayos J, Saxena K, Morra M, Sumegi J, Cantley LC, Terhorst C, Eck MJ. Crystal structures of the XLP protein SAP reveal a class of SH2 domains with extended, phosphotyrosine-independent sequence recognition. Mol Cell. 1999; 4:555–561. [PubMed: 10549287]
9. Shlapatska LM, Mikhalap SV, Berdova AG, Zelensky OM, Yun TJ, Nichols KE, Clark EA, Sidorenko SP. CD150 association with either the SH2-containing inositol phosphatase or the SH2-containing protein tyrosine phosphatase is regulated by the adaptor protein SH2D1A. J Immunol. 2001; 166:5480–5487. [PubMed: 11313386]
10. Chan B, Lanyi A, Song HK, Griesbach J, Simarro-Grande M, Poy F, Howie D, Sumegi J, Terhorst C, Eck MJ. SAP couples Fyn to SLAM immune receptors. Nat Cell Biol. 2003; 5:155–160. [PubMed: 12545174]
11. Katz G, Krummey SM, Larsen SE, Stinson JR, Snow AL. SAP facilitates recruitment and activation of LCK at NTB-A receptors during restimulation-induced cell death. J Immunol. 2014; 192:4202–4209. [PubMed: 24688028]
12. Cannons JL, Yu LJ, Hill B, Mijares LA, Dombroski D, Nichols KE, Antonellis A, Koretzky GA, Gardner K, Schwartzberg PL. SAP regulates T(H)2 differentiation and PKC-theta-mediated activation of NF-kappaB1. Immunity. 2004; 21:693–706. [PubMed: 15539155]
13. Nunez-Cruz S, Yeo WC, Rothman J, Ojha P, Bassiri H, Juntilla M, Davidson D, Veillette A, Koretzky GA, Nichols KE. Differential requirement for the SAP-Fyn interaction during NK T cell development and function. J Immunol. 2008; 181:2311–2320. [PubMed: 18684920]

14. Qi H, Cannons JL, Klauschen F, Schwartzberg PL, Germain RN. SAP-controlled T-B cell interactions underlie germinal centre formation. Nature. 2008; 455:764–769. [PubMed: 18843362]
15. Baldanzi G, Pighini A, Bettio V, Rainero E, Traini S, Chianale F, Porporato PE, Filigheddu N, Mesturini R, Song S, Schweighoffer T, Patrussi L, Baldari CT, Zhong XP, van Blitterswijk WJ, Sinigaglia F, Nichols KE, Rubio I, Parolini O, Graziani A. SAP-mediated inhibition of diacylglycerol kinase α regulates TCR-induced diacylglycerol signaling. J Immunol. 2011; 187:5941–5951. [PubMed: 22048771]
16. Olenchock BA, Guo R, Carpenter JH, Jordan M, Topham MK, Koretzky GA, Zhong XP. Disruption of diacylglycerol metabolism impairs the induction of T cell anergy. Nat Immunol. 2006; 7:1174–1181. [PubMed: 17028587]
17. Zhong XP, Hainey EA, Olenchock BA, Jordan MS, Maltzman JS, Nichols KE, Shen H, Koretzky GA. Enhanced T cell responses due to diacylglycerol kinase zeta deficiency. Nat Immunol. 2003; 4:882–890. [PubMed: 12883552]
18. She J, Matsui K, Terhorst C, Ju ST. Activation-induced apoptosis of mature T cells is dependent upon the level of surface TCR but not on the presence of the CD3 zeta ITAM. Int Immunol. 1998; 10:1733–1740. [PubMed: 9846702]
19. Sato M, Liu K, Sasaki S, Kunii N, Sakai H, Mizuno H, Saga H, Sakane F. Evaluations of the selectivities of the diacylglycerol kinase inhibitors r59022 and r59949 among diacylglycerol kinase isozymes using a new non-radioactive assay method. Pharmacology. 2013; 92:99–107. [PubMed: 23949095]
20. Issandou M, Bayard F, Darbon JM. Inhibition of MCF-7 cell growth by 12-O-tetradecanoylphorbol-13-acetate and 1,2-dioctanoyl-sn-glycerol: distinct effects on protein kinase C activity. Cancer Res. 1988; 48:6943–6950. [PubMed: 3180102]
21. Carrasco S, Merida I. Diacylglycerol-dependent binding recruits PKCtheta and RasGRP1 C1 domains to specific subcellular localizations in living T lymphocytes. Mol Biol Cell. 2004; 15:2932–2942. [PubMed: 15064353]
22. Spitaler M, Emslie E, Wood CD, Cantrell D. Diacylglycerol and protein kinase D localization during T lymphocyte activation. Immunity. 2006; 24:535–546. [PubMed: 16713972]
23. Chauveau A, Le Floc'h A, Bantilan NS, Koretzky GA, Huse M. Diacylglycerol kinase α establishes T cell polarity by shaping diacylglycerol accumulation at the immunological synapse. Sci Signal. 2014; 7:ra82. [PubMed: 25161317]
24. Quann EJ, Merino E, Furuta T, Huse M. Localized diacylglycerol drives the polarization of the microtubule-organizing center in T cells. Nat Immunol. 2009; 10:627–635. [PubMed: 19430478]
25. Ebinu JO, Stang SL, Teixeira C, Bottorff DA, Hooton J, Blumberg PM, Barry M, Bleakley RC, Ostergaard HL, Stone JC. RasGRP links T-cell receptor signaling to Ras. Blood. 2000; 95:3199–3203. [PubMed: 10807788]
26. Altman A, Villalba M. Protein kinase C-theta (PKCtheta): it's all about location, location, location. Immunol Rev. 2003; 192:53–63. [PubMed: 12670395]
27. Manicassamy S, Sun Z. The critical role of protein kinase C-theta in Fas/Fas ligand-mediated apoptosis. J Immunol. 2007; 178:312–319. [PubMed: 17182568]
28. Layer K, Lin G, Nencioni A, Hu W, Schmucker A, Antov AN, Li X, Takamatsu S, Chevassut T, Dower NA, Stang SL, Beier D, Buhlmann J, Bronson RT, Elkon KB, Stone JC, Van Parijs L, Lim B. Autoimmunity as the consequence of a spontaneous mutation in Rasgrp1. Immunity. 2003; 19:243–255. [PubMed: 12932358]
29. Chuck MI, Zhu M, Shen S, Zhang W. The role of the LAT-PLC-gamma1 interaction in T regulatory cell function. J Immunol. 2010; 184:2476–2486. [PubMed: 20130215]
30. Springael C, Thomas S, Rahmouni S, Vandamme A, Goldman M, Willems F, Vosters O. Rottlerin inhibits human T cell responses. Biochem Pharmacol. 2007; 73:515–525. [PubMed: 17141738]
31. Lenardo MJ. Interleukin-2 programs mouse alpha beta T lymphocytes for apoptosis. Nature. 1991; 353:858–861. [PubMed: 1944559]
32. Cheng LE, Chan FK, Cado D, Winoto A. Functional redundancy of the Nur77 and Nor-1 orphan steroid receptors in T-cell apoptosis. EMBO J. 1997; 16:1865–1875. [PubMed: 9155013]

33. Wang A, Rud J, Olson CM, Anguita J, Osborne BA. Phosphorylation of Nur77 by the MEK-ERK-RSK cascade induces mitochondrial translocation and apoptosis in T cells. J Immunol. 2009; 183:3268–3277. [PubMed: 19675165]

34. Smith JA, Poteet-Smith CE, Xu Y, Errington TM, Hecht SM, Lannigan DA. Identification of the first specific inhibitor of p90 ribosomal S6 kinase (RSK) reveals an unexpected role for RSK in cancer cell proliferation. Cancer Res. 2005; 65:1027–1034. [PubMed: 15705904]

35. Filipovich AH, Zhang K, Snow AL, Marsh RA. X-linked lymphoproliferative syndromes: brothers or distant cousins? Blood. 2010; 116:3398–3408. [PubMed: 20660790]

36. Wu C, Nguyen KB, Pien GC, Wang N, Gullo C, Howie D, Sosa MR, Edwards MJ, Borrow P, Satoskar AR, Sharpe AH, Biron CA, Terhorst C. SAP controls T cell responses to virus and terminal differentiation of TH2 cells. Nat Immunol. 2001; 2:410–414. [PubMed: 11323694]

37. Czar MJ, Kersh EN, Mijares LA, Lanier G, Lewis J, Yap G, Chen A, Sher A, Duckett CS, Ahmed R, Schwartzberg PL. Altered lymphocyte responses and cytokine production in mice deficient in the X-linked lymphoproliferative disease gene SH2D1A/DSHP/SAP. Proc Natl Acad Sci U S A. 2001; 98:7449–7454. [PubMed: 11404475]

38. Dominguez CL, Floyd DH, Xiao A, Mullins GR, Kefas BA, Xin W, Yacur MN, Abounader R, Lee JK, Wilson GM, Harris TE, Purow BW. Diacylglycerol kinase α is a critical signaling node and novel therapeutic target in glioblastoma and other cancers. Cancer Discov. 2013; 3:782–797. [PubMed: 23558954]

39. Quann EJ, Liu X, Altan-Bonnet G, Huse M. A cascade of protein kinase C isozymes promotes cytoskeletal polarization in T cells. Nat Immunol. 2011; 12:647–654. [PubMed: 21602810]

40. Gharbi SI, Rincón E, Avila-Flores A, Torres-Ayuso P, Almena M, Cobos MA, Albar JP, Mérida I. Diacylglycerol kinase ζ controls diacylglycerol metabolism at the immunological synapse. Mol Biol Cell. 2011; 22:4406–4414. [PubMed: 21937721]

41. Moran AE, Holzapfel KL, Xing Y, Cunningham NR, Maltzman JS, Punt J, Hogquist KA. T cell receptor signal strength in Treg and iNKT cell development demonstrated by a novel fluorescent reporter mouse. J Exp Med. 2011; 208:1279–1289. [PubMed: 21606508]

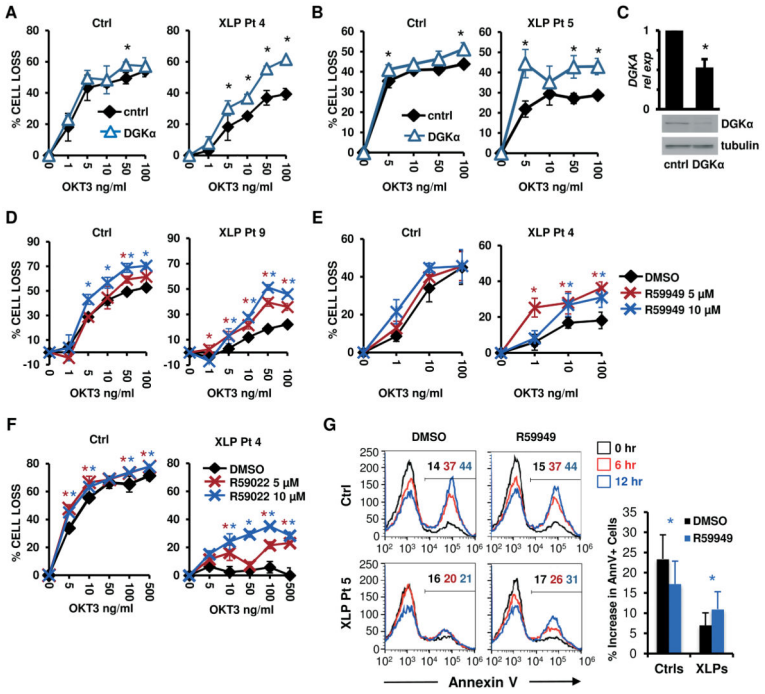

Figure 1. DGKα silencing or inhibition restores RICD in XLP-1 patient T cells

(A–B) Activated T cells from normal donors (Ctrl) or indicated XLP-1 patients were transfected with control (cntrl) or DGKα-specific siRNA, then restimulated 4 days later with OKT3 Ab. After 24 hours, % cell loss was evaluated by PI staining. Data are mean ± SD of 2 experiments (A) or 1 experiment (B) performed in triplicate, representative of 2 independent experiments using different control donors.

(C) DGKα relative expression (rel exp) in siRNA-transfected cells from (A) measured by qRT-PCR (upper panel, mean ± SEM, n=4) or by Western blotting, with tubulin as loading control (lower panel).

(D–F) Ctrl or XLP patient T cells were restimulated with OKT3 Ab following pretreatment with DGK inhibitors R59949 or R59022 (5–10 μM), or DMSO. After 24 hours, % cell loss was evaluated by PI staining. Data are mean ± SD of 3 experiments (E), or 1 experiment (D, F) performed in triplicate representative of 2 independent experiments using different control donors.

(G) Cells used in (D) were pre-treated with R59949 (10 μM) or DMSO and restimulated with OKT3 (100 ng/ml) for 0, 6 and 12 hours. The % of apoptotic cells was measured by AnnexinV staining. Representative histograms are shown; marker numbers denote % AnnexinV$^+$ cells. The net increase in AnnexinV$^+$ cells at 12 hours is shown at right. Data are mean ± SD of 6 independent experiments using 4 separate controls and 2 XLP patients. Asterisks denote statistical significance by two-way ANOVA with Sidak correction (A–B, D–F) or paired t-test (C, G).

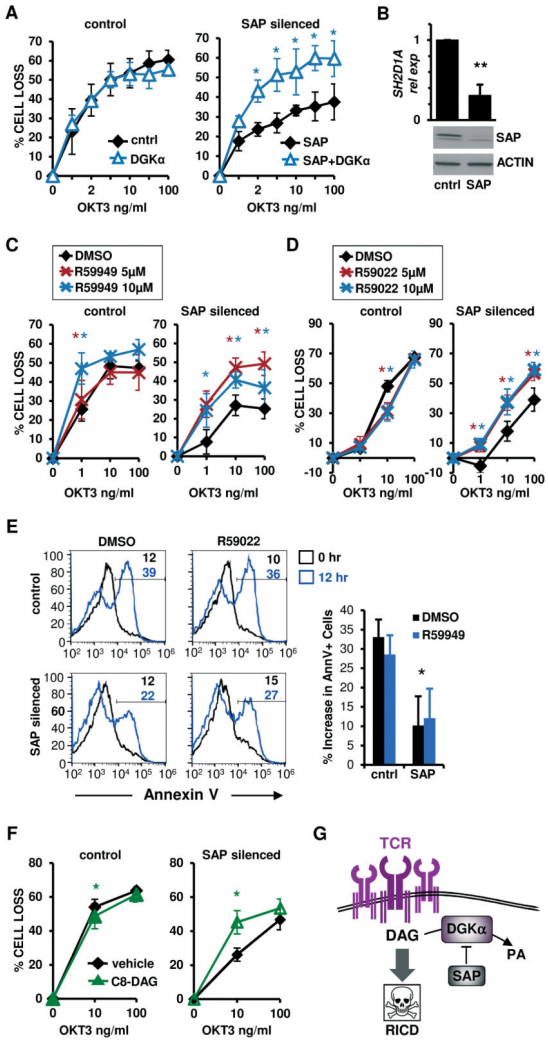

Figure 2. DGKα silencing or inhibition restores RICD in SAP-silenced T cells

(A) Activated normal donor T cells were transfected with control or SAP siRNA and restimulated 4 days later with OKT3 Ab. After 24 hours, % cell loss was evaluated by PI staining. Data are mean ± SEM of 3 experiments performed in triplicate.

(B) SAP expression in siRNA-transfected T cells from (A) was measured by qRT-PCR (upper panel, mean ± SEM of 4 experiments) or by Western blotting, with actin as a loading control (lower panel).

(C–D) siRNA-transfected cells (A) were restimulated with OKT3 Ab following pretreatment with DMSO, DGK inhibitor R59949 or R59022 (5–10 μM). After 24 hours, the % cell loss was evaluated by PI staining. Data are mean ± SEM of 5 experiments (C), or 5 (control) and 8 (SAP siRNA) independent experiments (D) performed in triplicate.

(E) siRNA-transfected cells as in (A) were pretreated with DMSO or R59022 (10 μM) and restimulated with OKT3 (10 ng/ml). After 12 hours, the % apoptotic cells was evaluated by AnnexinV staining. Representative histograms are shown; marker numbers denote % AnnexinV$^+$ cells. The net increase in AnnexinV$^+$ cells at 12 hours is shown at right. Data are mean ± SD of 4 experiments.

(F) siRNA-transfected cells (A) were treated with C8-DAG (50 μM) and restimulated with OKT3 Ab. After 24 hours, % cell loss was evaluated by PI staining. Data are mean ± SEM of 5 experiments performed in triplicate. Asterisks denote statistical significance by two-way ANOVA with Sidak correction (A,C,D–F) or paired t-test (B,E).

(G) Schematic cartoon: pro-apoptotic TCR signaling is governed by DGKα inhibition in activated T cells.

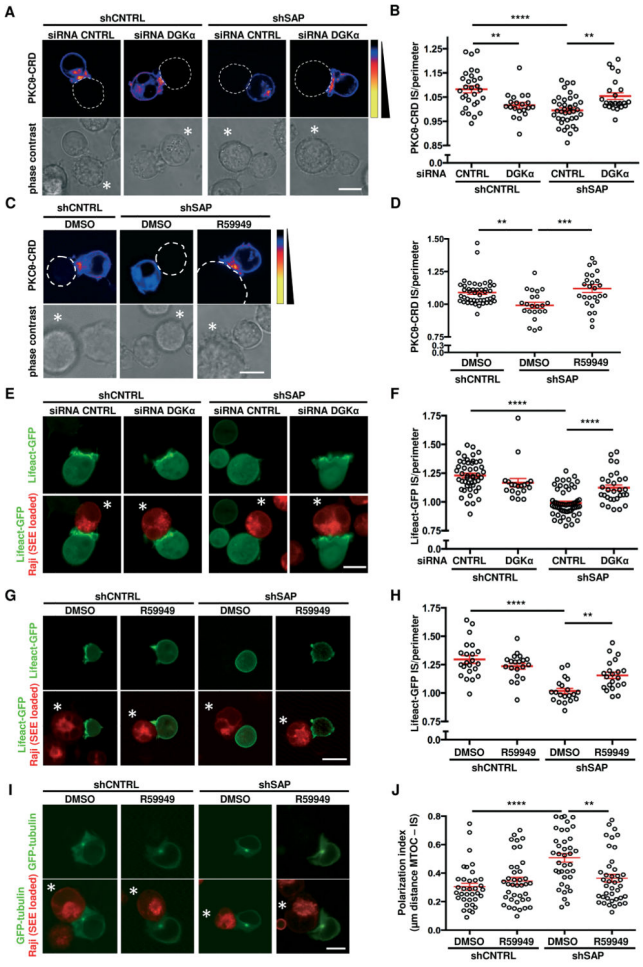

Figure 3. DGKα silencing or inhibition restores synapse formation in SAP-deficient T cells

ShCNTRL or shSAP Jurkat T cells were transiently transfected as indicated. After 48 (C, D, G, H, I, J) or 96 (A, B, E, F) hours, T cells were challenged with SEE-loaded Raji B cells, and confocal live cell images were captured during T cell-APC conjugation. In (C, D, G, H, I, J) T cells were pretreated for 30 minutes with 10 μM R59949 or DMSO.

(A, C) Top row: EGFP-tagged PKCθ-CRD (pseudo color) together with the perimeter of the APC (dotted line). Bottom row: phase contrast images with APC denoted by *. Scale bar 10 μm.

(B, D) Quantification of EGFP-PKCθ-CRD accumulation at the IS. Mean ± SEM of >20 conjugates per condition from 3 experiments.

(E, G) Top row: Lifeact-GFP (green). Bottom row also shows Raji B cells stained with CellTracker Red CMTPX (red). Scale bar 10 μm.

(F, H) Quantification of Lifeact-GFP accumulation at the IS. Mean ± SEM of >20 conjugates per condition from 3 experiments.

(I) Top row: GFP-tubulin (green). Bottom row also shows Raji B cells stained with CellTracker Red CMTPX (red). Scale bar 10 μm.

(J) Quantification of MTOC polarization index. Mean ± SEM of >35 conjugates per condition from 2 experiments. Asterisks in all panels denote statistical significance by one-way ANOVA with Sidak correction.

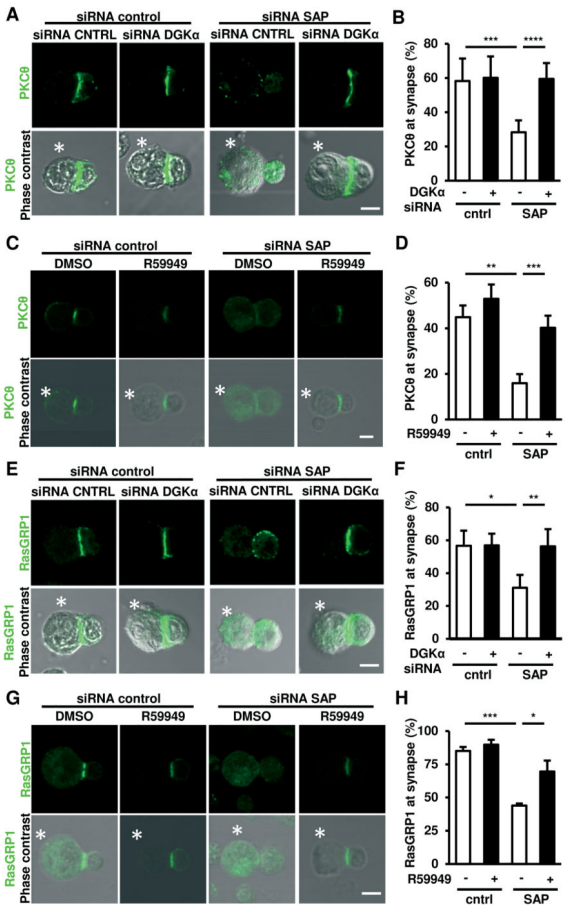

Figure 4. DGKα silencing or inhibition restores PKCθ and RasGRP1 recruitment to the IS in SAP-deficient cells

(A, C, E, G) Activated T cells were transfected with the indicated siRNA and after 72 hours incubated with SEE-loaded Raji B cells (denoted with *) for 15 minutes, fixed and stained for PKCθ (A,C) or RasGRP1(E,G). Top rows: target protein (green), bottom rows also show phase contrast. Scale bar 5 μm.

(B) Percentage of cells displaying PKCθ at the IS. Data are mean ± SEM of 6 replicates from 2 independent experiments.

(D) Percentage of cells displaying PKCθ at the IS. Data are mean ± SEM of 3 experiments.

(F) Percentage of cells with RasGRP1 at the IS. Data are mean ± SD of 1 representative experiment performed in quadruplicate.

(H) Percentage of cells displaying RasGRP1 at the IS. Data are mean ± SEM of 3 experiments. Asterisks in all panels denote statistical significance by two-way ANOVA + Sidak correction.

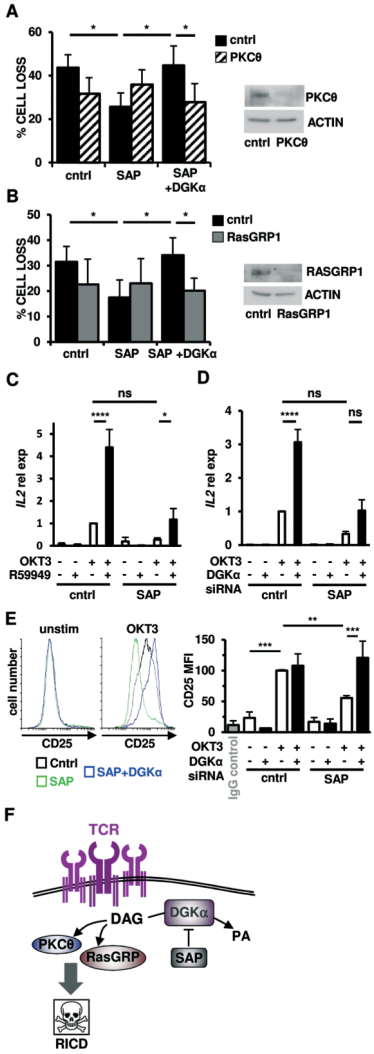

Figure 5. DGKα silencing restores TCR-induced PKCθ and Ras-mediated signaling pathways to drive RICD in SAP-deficient cells

(A-B) Activated normal donor T cells were transfected with the indicated siRNA and restimulated 4 days later with OKT3 Ab (10 ng/ml). After 24 hours, % cell loss was evaluated by PI staining. Data are mean ± SEM of 7 (A) or 6 (B) experiments performed in triplicate. Right panels: expression of PKCθ (A) or RasGRP1 (B) was measured by Western blotting, with actin as a loading control.

(C–D) Quantitative RT-PCR for *IL2* mRNA in T cells pre-treated with R59949 (10 μM) (C) or transfected with DGKα siRNA (D) after restimulation with OKT3 (10 μg/ml, 4 hours) *GUSB* served as the reference gene. Graphs represent mean ± SEM of 6 (C) or 7 (D) experiments.

(E) Left: Representative flow cytometric histograms showing CD25 surface expression on siRNA-transfected T cells from (A) ± OKT3 restimulation (24 hours). Right: graph depicts mean fluorescence intensity (MFI) of CD25 expression. Data are mean ± SEM of 4 experiments. Asterisks in all panels denote statistical significance by two-way ANOVA with Sidak correction.

(F) Schematic cartoon: SAP-mediated inhibition of DGKα activity ensures a sufficient pool of DAG required for proper IS organization and recruitment of PKCθ and RasGRP, which mediates downstream signaling for RICD.

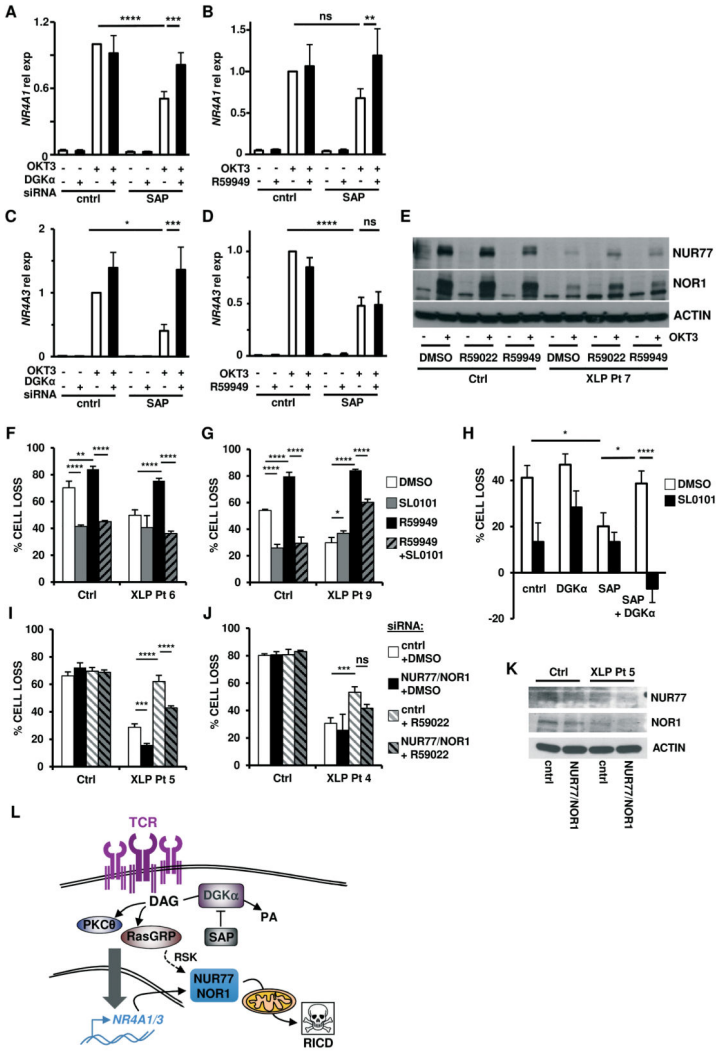

Figure 6. Silencing or inhibition of DGKα restores RICD sensitivity in SAP-deficient T cells via induction of pro-apoptotic molecules NUR77 and NOR1

(A–D) Quantitative RT-PCR for *NR4A1* (A–B) or *NR4A3 (C-D)* from activated normal donor T cells transfected with control or SAP-specific siRNA ± DGKα-specific siRNA (A,C) or 5 μM R59949 (B,D) and restimulated with OKT3 (10 μg/ml) for 4 hours. *GUSB* served as the reference gene. Data are mean ± SEM of 8 (A), 5 (B), 7 (C) or 6 (D) experiments.

(E) Activated T cells from normal donor (Ctrl) or XLP-1 patient 7 were pretreated for 30 minutes with R59022 or R59949 (10 μM), then restimulated with 100 ng/ml OKT3. Cells lysates were analyzed by Western blotting for NUR77, NOR1 and β-actin content. Data are representative of 2 independent experiments using different donors.

(F–G) Activated T cells from normal donors (Ctrl) or XLP-1 patients were pretreated for 30 minutes with DMSO, SL0101-1 (90 μM), R59949 (10 μM), or both, followed by restimulation with OKT3 (100 ng/ml). After 24 hours, % cell loss was evaluated by PI staining. Data are mean ± SD of 1 experiment each performed in triplicate using different donors.

(H) Activated donor T cells were transfected with the indicated siRNA and treated 4 days later with SL0101-1 (50 μM) for 30 minutes, followed by OKT3 (10 ng/ml). After 24 hours, % cell loss was evaluated by PI staining. Data are mean ± SEM of 5 experiments performed in triplicate.

(I–J) Activated T cells from normal donors (Ctrl) or XLP-1 patients were transfected control or NUR77+NOR1 siRNA and treated 4 days later with DMSO or R59022 (10 μM) for 30 minutes, followed by OKT3 (100 ng/ml). After 24 hours, % cell loss was evaluated by PI staining. Data are mean ± SD of 1 experiment each, performed in triplicate using different donors. Asterisks in all panels denote statistical significance by two-way ANOVA with Sidak correction.

(K) Western blot for NUR77 and NOR1 expression in OKT3-restimulated, siRNA-transfected T cells from (I). Actin served as a loading control.

(L) Schematic cartoon: mechanism of pro-apoptotic TCR signaling governed by SAP-dependent DGKα inhibition in activated T cells.

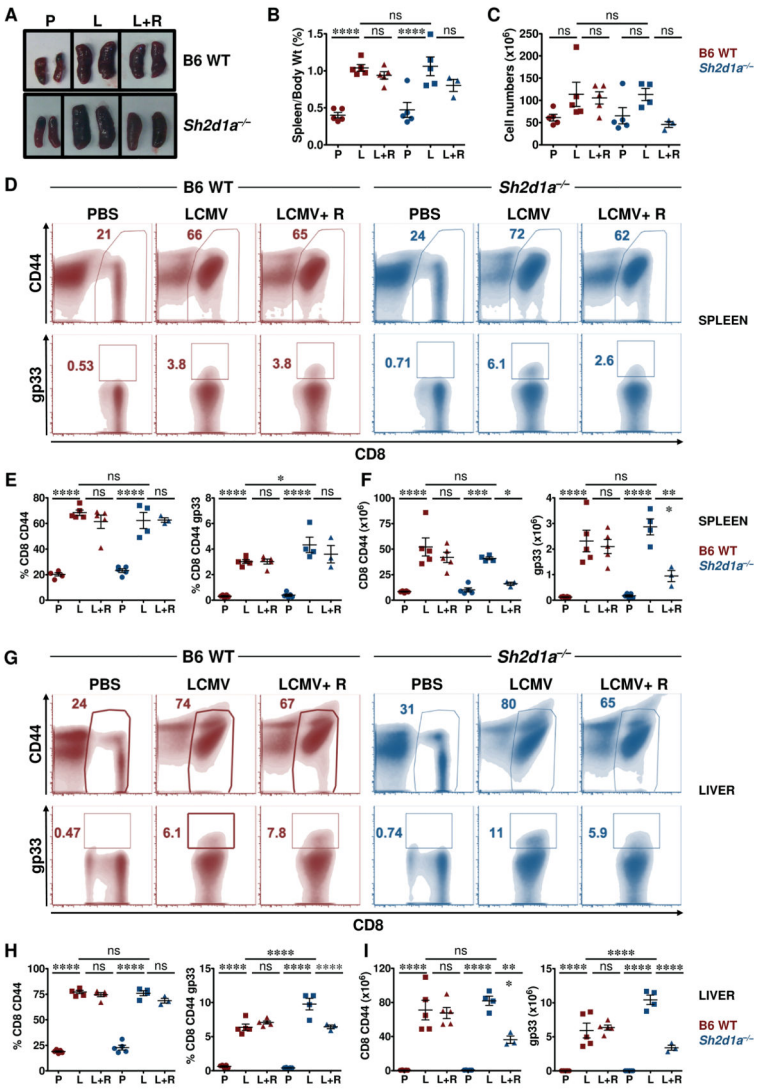

Figure 7. R59022 DGK inhibitor reduces the numbers of activated virus- specific CD8$^+$ T cells in LCMV-infected *Sh2d1a*$^{-/-}$ mice

(A) Images of spleens from uninfected (PBS, "P") and LCMV infected mice without (LCMV, "L") or with R59022 treatment (LCMV+R59022, "L+R"). Representative spleens from each cohort from B6 WT (top panel) and *Sh2d1a*$^{-/-}$ mice (lower panel) are shown. **(B)** Ratio of spleen over body weight and **(C)** total splenocyte count for animals in each group are presented. B6 WT mice = red symbols, *Sh2d1a*$^{-/-}$ mice = blue symbols. **(D–I)** Representative flow cytometric (density) plots showing the percentages of CD8$^+$ CD44$^+$ (top) and LCMV-specific CD8$^+$ gp33$^+$ (bottom) in the spleens **(D)** and livers **(G)** of B6 WT and *Sh2d1a*$^{-/-}$ mice. Percentages **(E, H)** and absolute numbers **(F, I)** of CD8$^+$ CD44$^+$ and CD8$^+$ CD44$^+$ gp33$^+$ cells in the spleens **(E, F)** and livers **(H, I)** of B6 WT (red symbols) and *Sh2d1a*$^{-/-}$ (blue symbols) mice.

Data are from 1 of 2 experiments in which a total of 6–10 mice in each cohort was examined. Error bars represent SD. Asterisks denote statistical significance that was determined by two-way ANOVA with Sidak correction. ns: not significant.

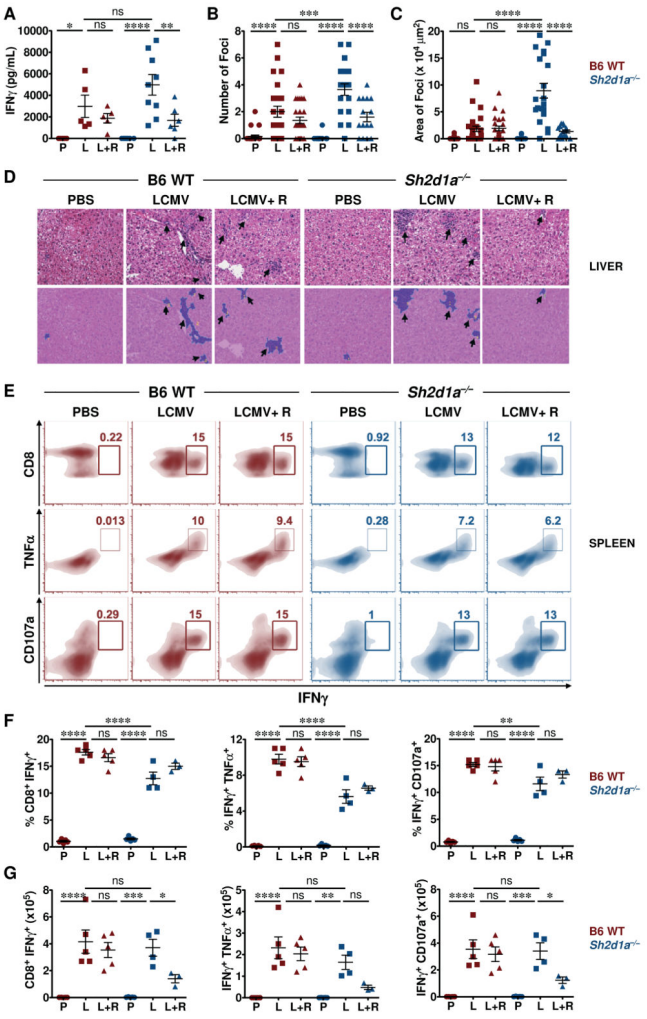

Figure 8. R59022 DGK inhibitor reduces the numbers but not incidence of virus-specific activated CD8$^+$ cytokine producing cells in the spleens of LCMV infected *Sh2d1a*$^{-/-}$ mice

B6 WT (red symbols) and *Sh2d1a*$^{-/-}$ mice (blue symbols) were either uninfected (PBS, “P”) or infected with LCMV without (LCMV, “L”) or with R59022 treatment (LCMV+R59022, “L+R”).

(A) Serum IFNγ levels were assayed on day 8 post-infection by ELISA. Data are compiled from 2 experiments in which a total of 6–10 mice in each cohort were examined. Error bars represent SEM.

(B–D) H&E-stained liver sections from mice in each group were analyzed for the number of inflammatory foci **(B)** and area of the inflammatory infiltrate **(C)**. For each sample, five random fields were captured at 20X magnification and scored. Histology of livers from representative mice in each group under 20X magnification (top row) is shown **(D)**. Arrows point to the inflammatory foci. Micrographs in the bottom row are the respective analyzed images shown in the top row.

(E–G) Splenocytes (2×10^6) from PBS (P), LCMV-infected (L) and LCMV-infected mice with R59022 treatment (L+R) groups were left unstimulated or stimulated with 0.4 ng/mL gp33 peptide in the presence of 1000 μg/mL monensin for 5 hours. Cells were then analyzed

for intracellular cytokine production and degranulation. Representative flow cytometric (density) plots gated on $CD8^+$ $CD44^+$ splenocytes showing the percentages of $CD8^+$ $IFN\gamma^+$ (top), IFNγ+ $TNF\alpha^+$ (middle) and $IFN\gamma^+$ $CD107a^+$ (bottom) cells from B6 WT and *Sh2d1a* / mice **(E)**. Percentages **(F)** and absolute numbers **(G)** of $CD8^+$ $IFN\gamma^+$, $IFN\gamma^+$ $TNF\alpha^+$ and $IFN\gamma^+$ $CD107a^+$ cells. Absolute numbers were calculated by multiplying the percentages with the respective absolute numbers of $CD8^+$ $gp33^+$ cells.

Error bars in **B, C, F,** and **G** represent SD. Asterisks denote statistical significance that was determined by two-way ANOVA with Sidak correction. ns: not significant.